PP/EVA Blends: Mechanical Properties and Morphology. Effect of Compatibilizers on the Impact Behavior

ALFREDO MACIEL, VERÓNICA SALAS, OCTAVIO MANERO

Instituto de Investigaciones en Materiales, Circuito Exterior de Ciudad Universitaria, Universidad Nacional Autónoma de México, Delegación, Coyoacán, Apdo. Postal 70-360, México, D.F., México

Received: September 25, 2004

ABSTRACT: The mechanical properties of blends of isotactic polypropylene (PP) and poly[ethylene-*co*-(vinyl acetate)] (EVA) are studied under tension at several temperatures (from –30°C to room temperature). The morphology and thermal properties are given attention at every stage of the stretching process. To improve the impact resistance of the blends, poly[propylene-*graft*-(maleic anhydride)] (PPMA) and hydroxylated EVA (EVAOH) are used as compatibilizers. The domain size of the dispersed phase decreases with compatibilizer content, improving the impact resistance of the blends. This is accompanied with changes in the morphology of such systems. © 2005 Wiley Periodicals, Inc. Adv Polym Techn 24: 241–252, 2005; Published online in Wiley InterScience (www.interscience.wiley.com). DOI 10.1002/adv.20050

KEY WORDS: Compatibilization, Deformation, Morphology, Polypropylene

Introduction

Polypropylene (PP) presents brittleness, low mechanical performance, and low impact resistance at temperatures below or around its glass transition temperature (T_g). This is the reason and motivation to make PP blends with elastomeric compounds. For example, PP increases notably its impact resistance at temperatures between −120°C and 20°C when blended with EPDM[1–5] and SBR.[5] The brittle–ductile transition of PP/EPR blends has been given attention.[6–10] Better impact and mechanical properties obtained at temperatures between

Correspondence to: Alfredo Maciel; e-mail: macielal@servidor.unam.mx.

Advances in Polymer Technology, Vol. 24, No. 4, 241–252 (2005)

−190°C and −30°C have been reported in PP/SEBS blends.[11] At low temperatures, impact resistance of PP is greatly increased in blends with poly[ethylene-*co*-(vinyl acetate)] (EVA).[12–15] Dynamic-mechanical analysis and morphology studies of PP/EVA blends reveal two glass transitions and phase separation,[16] but recently, miscibility at high EVA contents was reported.[17] LDPE has been employed to promote miscibility in the PP/EVA blends.[18] Interpenetrated networks have been found in PP/EVA blends where the EVA phase has been extracted using toluene.[13] Similar systems were found in EVA/LDPE blends.[19]

To induce compatibility in PP physical blends, PP has been grafted with several compounds, one among them is maleic anhydride.[20,21] The more reacting PP has been used as adhesive among polymer layers.[22] PP grafted with acrylic acid has also been used as compatibilizer.[23,24] EPDM grafted with maleic anhydride has been used in blends with PP to reduce the size of the dispersed phase and hence to increase the impact resistance.[25] Similarly, EPR grafted with maleic anhydride has been used in blends with PP to increase the impact properties of PP.[26] PP/EVA blends have been treated with amino acids and with EVA-SH to induce compatibility.[27,28]

With respect to the mechanism of deformation under tension of polymer blends, this is strongly related to the behavior of the microdomains and their adhesion to the matrix. Studies on the mechanism of deformation and its relation with morphological changes under tension have been performed in nylon-6/PP blends[29] and grafted EPR with maleic anhydride.[30] In the PP/epoxy resins blend, the formation of microcavities under tension tests is responsible for the propagation of fractures.[31–33] Additional evidence of the relation between adhesive failure and the generation of cavities has been observed in the PVC/NBR blends[34] and in the PP/fillers system.[35]

In this work, we relate the morphological changes of the PP/EVA blend under tension at various temperatures (−30°C to room temperature) and their effects on the thermal properties. The effect of the use of compatibilizers on the impact properties is also analyzed.

Experimental Part

Isotactic polypropylene (profax 6523) from Himont with $M_w = 228{,}400$ g/mol and $M_n = 28{,}900$ g/mol melt flow index = 4, glass transition temperature = −11°C, melting temperature = 173°C, and density of 0.9 g/cm^3 was used in the blends. Poly[ethylene-*co*-(vinyl acetate)], with 28% of vinyl acetate content, $M_w = 125{,}690$ g/mol and $M_n = 47{,}950$ g/mol, melt flow index = 7, glass transition temperature = −37°C, melting temperature = 76°C, and density of 0.95 g/cm^3 was also used. Molecular weights were determined in a Waters 150°C GPC using trichlorobenzene as solvent at 120°C. Calibration was made with ten polystyrene standards from 10,000 to 2,700,000 g/mol at 135°C. The thermal properties were measured in a Dupont 910 DSC. PP/EVA compositions considered were 100/0, 90/10, 80/20, 70/30, 60/40, 50/50, 40/60, 30/70, 20/80, and 0/100.

The pellets of PP and EVA were premixed as received before adding to a screw extruder. The blends were prepared according to two procedures: a Haake 254 single-screw extruder with $L/D = 25{:}1$ and 71 cm length was used with feed-die temperature profile of 210, 220, 220, and 225°C. After the first extrusion process, pellets were fed again into the extruder for another extrusion cycle (P1). The second procedure (P2) involved extrusion in a twin-screw extruder (Haake TW-100) followed by extrusion in the single-screw extruder of the pellets. A Demag Ergo-Tech 50–200 injection-molding machine was used to prepare the samples for mechanical, impact, and morphological studies. The cooling water temperature was 15°C with a cooling time of 20 s.

Some samples were prepared using poly[propylene-*graft*-(maleic anhydride)] (PPMA) with MA content of 0.86% and hydroxylated poly[ethylene-*co*-(vinyl acetate)] (EVAOH) with 42.5% of hydroxy groups to form a compatibilizer in situ. PPAM was synthesized by Industrias Resistol, S.A.,[35] and kindly provided for this research. EVAOH was synthesized in our laboratory and reported previously.[36] Two compositions were used: the first included 12 g of PPMA and 50 g of EVAOH per 1000 g of the PP/EVA blend, which renders 6.2 phr compatibilizer content. This corresponds to 1.2 phr PPMA and 5 phr EVAOH, which yields the ratio of 17 hydroxy groups per MA group. The second included 10 phr EVAOH with respect to the EVA content and 10 phr PPMA with respect to the PP content, which renders 10 phr compatibilizer content. All the blends were prepared according to the procedure (P2) described previously. Resulting PP/EVA compositions were 80/20, 60/40, 50/50, 40/60, and 20/80. The reaction between PPAM and EVAOH was followed by infrared spectroscopy with a Nicolet 510P instrument.

Tension tests were carried out at room temperature (21°C), 0, −15, and −30°C in an Instron 1125 machine according to the ASTM D 1708 norm at a speed of 100 mm/min. A temperature-controlled chamber (Instron 3111-001) was used in the tests. Three different strained samples were obtained for morphology studies: first taken at the yield point, a second one taken at 1/3 of total strain, and a third one taken at 2/3 of the total strain. Izod impact tests were carried out in notched specimens according to the ASTM D 256 norm.

Microscopy studies were carried out on the strained samples. Observations covered the front, inner, and fracture surfaces. The inner surface was uncovered by breaking the sample along the direction of deformation after immersion in liquid nitrogen for 3 min. Observations of fractured surfaces with EVA contents of 40% and 50% required further preparation consisting in the extraction of the EVA domains from the PP matrix using toluene for 48 h at room temperature. A gold-coating process was carried out before scanning microscopy observations (Leica Stereoscan 440). The micrographs were analyzed with an Image Pro Plus 3.0 software.

Thermal properties of samples were determined before and after tension tests. A DSC 2910 from TA Inst. was used with 7 mg sample cut within the strained zone 0.5 cm away from the fracture zone. They were heated at 10°C/min under nitrogen.

Results

MECHANICAL PROPERTIES OF THE PP/EVA BLENDS

Figures 1a–1c show the mechanical behavior under tension of the blends with varying composition and temperature. In Fig. 1a, the stress–strain curves for several compositions at room temperature depict a behavior that gradually changes. The curves for pure PP and blends with large concentration of PP present a peak at low deformations. For EVA and its blends, the initial stress is small and increases as the deformation augments. Figures 1b and 1c show the stress–strain curves at low temperatures for EVA contents of 60% and 80%. Blends present similarities with pure PP at low temperatures, with the presence of a peak at low strains and a transition to ductile behavior as temperature increases.

Figure 2 shows data of strain at break as a function of composition. Up to 70% EVA content, data lie

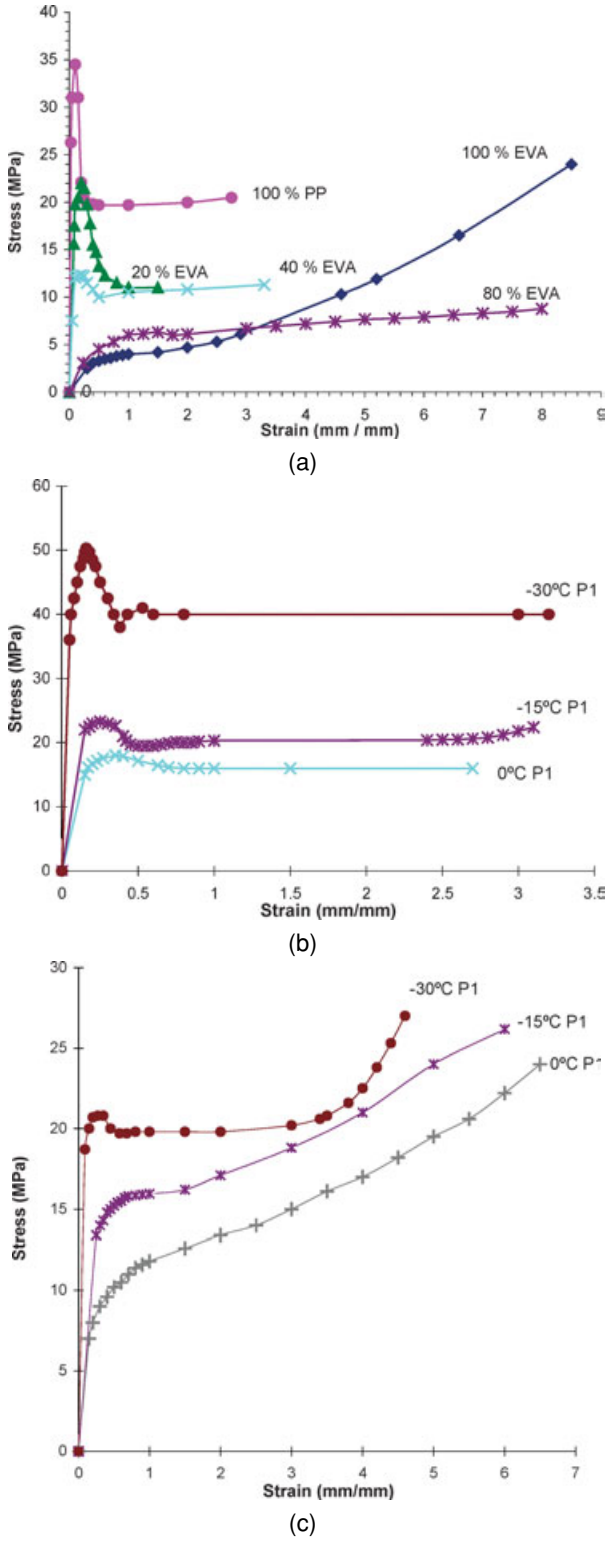

FIGURE 1. (a) Mechanical behavior in tension of PP, EVA along with their blends. (b) Stress–strain behavior of 40/60 PP/EVA blend deformed at 0, −15, and −30°C. (c) Stress–strain behavior of 20/80 PP/EVA blend deformed at 0, −15, and −30°C.

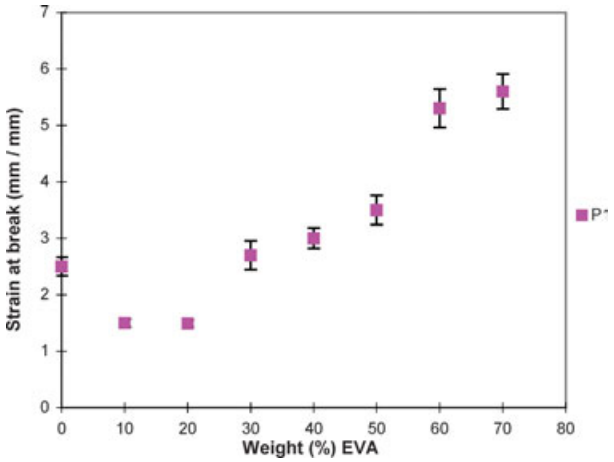

FIGURE 2. Strain at break point against composition at room temperature for PP/EVA blends made with procedure P1.

below the ideal mixing rule:

$$\varphi A = A_1\varphi_1 + A_2\varphi_2 + \cdots + A_n\varphi_n \qquad (1)$$

where A, A_1, A_2, A_n are a specific property and φ, φ_1, φ_2, φ_n are the volume fraction, respectively, of each polymer in the blend. For higher EVA contents, the strain at break follows closely the ideal mixing rule.

The elastic modulus increases with decreasing test temperature, and with decreasing EVA content, as shown in Fig. 3. At all temperatures, for strains higher than that of the yield point, the sample under tension becomes stress whitened, attributed to the formation of cavities.[4,11,34,36,37] This is accompanied with domains deformation, as observed in other semicrystalline polymers. Up to the peak of the stress versus strain curve (yield point), the dispersed phase has a spherical shape, but for higher strains, the domains become ellipsoidal. The domain deformation observed for this system is similar to the deformation of the spherulites in the well-known mechanism of deformation of semicrystalline polymers.[38,39] In what follows, we perform a morphological study on the changes of the microstructure of the blend as it is deformed by tension.[40]

Observations by electron microscopy on the blend samples reveal that the deformation of the dispersed phase is not uniform across the transversal direction of deformation. Originally, before deformation, the morphology of the blends obtained by extrusion had deformed domains along the extrusion direction. The aspect ratio was 1.5 (Fig. 4). Micrographs show that, after the strain is applied, the deformation of the domains in the center of the sample is larger than that in the edges. For example, Figs. 5a and 5b taken in the 20/80 PP/EVA content (room temperature) after 100% strain reveal that the domains in the center have an aspect ratio of 2.9, whereas for those in the edges the aspect ratio is 1.74. In Figs. 5c and 5d, the same situation prevails at −15°C. Domains in the center have an aspect ratio of 2.7, whereas for those in the edges this is 2.3.

As the deformation is increased to 1/3 of the total deformation (before rupture), corresponding to 270% strain at room temperature, the deformation of the domains in the center is more than twice that in the edges (aspect ratios are 1.8 and 4.3, respectively). As observed in Figs. 6a and 6b, at this strain the domains present adhesive failure, with voids in the interface with the matrix. This situation induces cavitation in the matrix, and the samples become stress whitened.

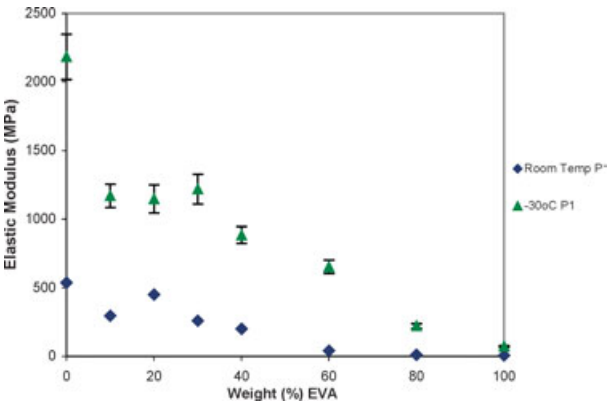

FIGURE 3. Elastic modulus with blend composition for PP/EVA blends at room temperature (◆) and −30°C (▲), made with procedure 1.

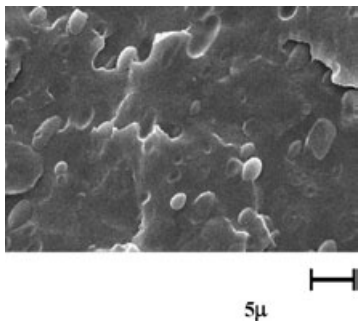

FIGURE 4. Morphology of the blend 20/80 PP/EVA before deformation.

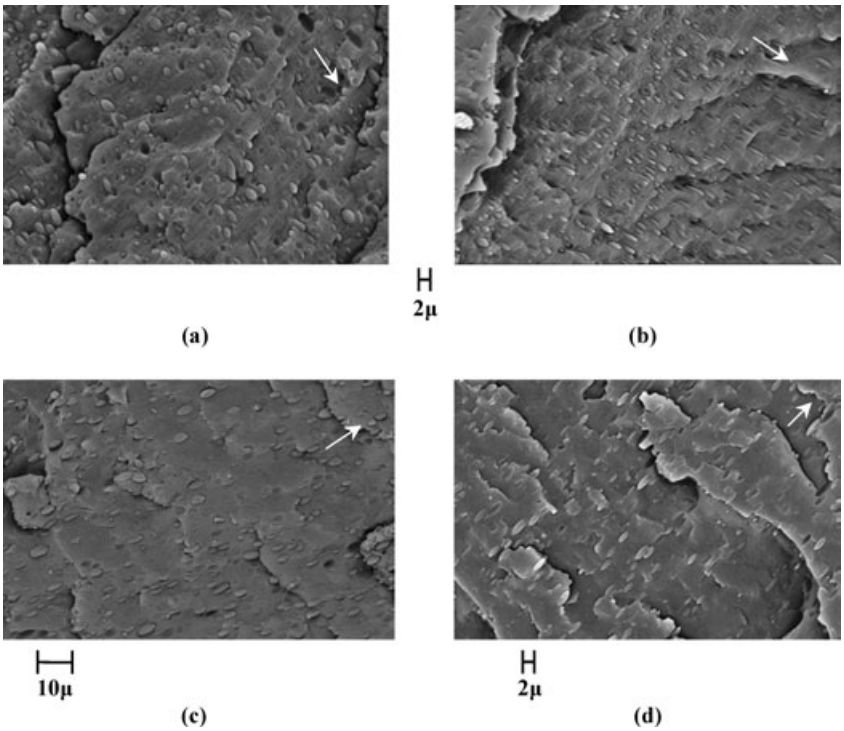

FIGURE 5. Morphology of the blend 20/80 PP/EVA after 100% strain at room temperature (a) edge and (b) center. At −15°C, (c) edge and (d) center.

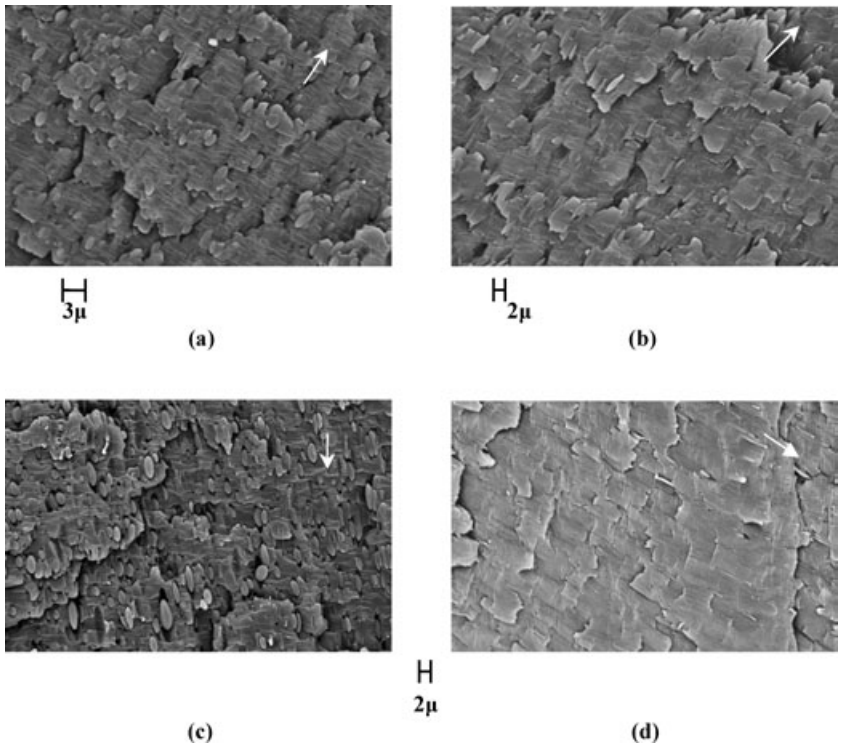

FIGURE 6. Morphology of the blend 20/80 PP/EVA after 270% strain at room temperature (a) edge and (b) center. At −15°C, (c) edge and (d) center.

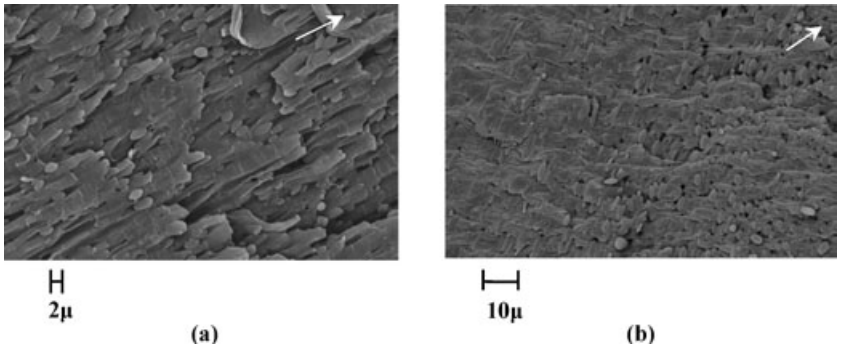

FIGURE 7. Morphology of the blend 20/80 after 500% strain at room temperature (a) and after 400% at −15°C (b).

At −15°C, where the strain is 200% (1/3 of the total strain at this temperature), the aspect ratio of the domains at the edges is 2.9 with lack of adhesion to the matrix (see Fig. 6c). In the center (Fig. 6d) deformation of the PP domains is very large, with a filament-like shape.

When the strain is 2/3 of the total strain, corresponding to 500% strain at room temperature, the domains in the center and in the edges do not deform due to adhesive failure with the matrix, as shown in Fig. 7a. At −15°C (also 2/3 of the total strain) corresponding to 400% strain, Fig. 7b shows the two regions (center and edge). In the center, the domains have a filament-like shape, whereas those in the edges have ellipsoidal shapes, separated from the matrix.

An interesting observation is shown in Fig. 8, where the same blend (20/80 PP/EVA) at 0°C taken on the surface at the rupture point (strain at break = 655%) presents elongated domains in the direction of the deformation by tension. The fibers have a width of 1.2 μm and show fractures propagating along the transversal direction. The formation of this type of microstructure under tension is similar to that presented in polyethylene blends (HDPE and LLDPE).[41]

THERMAL ANALYSIS

Figure 9 shows DSC data of EVA and PP/EVA blends. An endotherm at 48°C was noticed, corresponding to the melting enthalpy of the crystalline region of the PE section in the EVA copolymer.[42] This endotherm is present also in the 40/60 PP/EVA blend (upper line). At 76°C, a second crystalline region is noticed, corresponding to the EVA copolymer. The endotherm at 173°C is assigned to the PP of the blend.

To investigate further the characteristics of the first crystalline region, a thermal treatment was carried out. Samples were heated up to 250°C and rapidly quenched in liquid nitrogen. A DSC scan was then performed increasing the temperature from

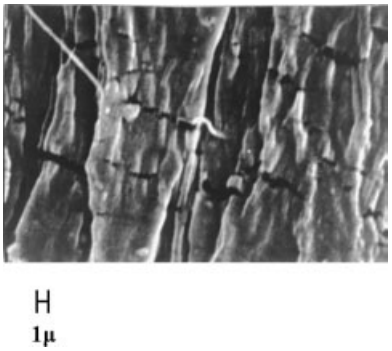

FIGURE 8. External morphology of the blend 20/80 PP/EVA at the rupture point (655% strain) tested at 0°C.

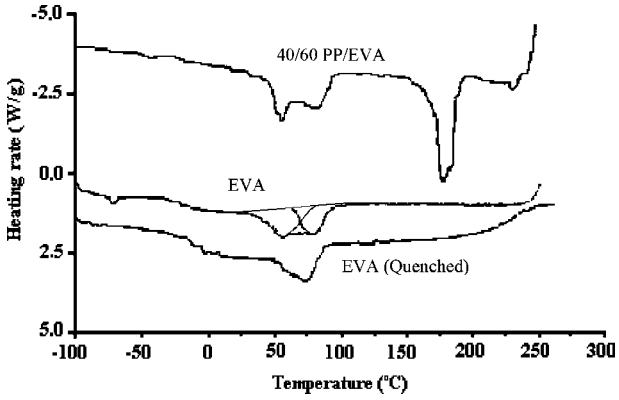

FIGURE 9. DSC thermogram of 40/60 PP/EVA blend, pure EVA, and quenched EVA in liquid nitrogen.

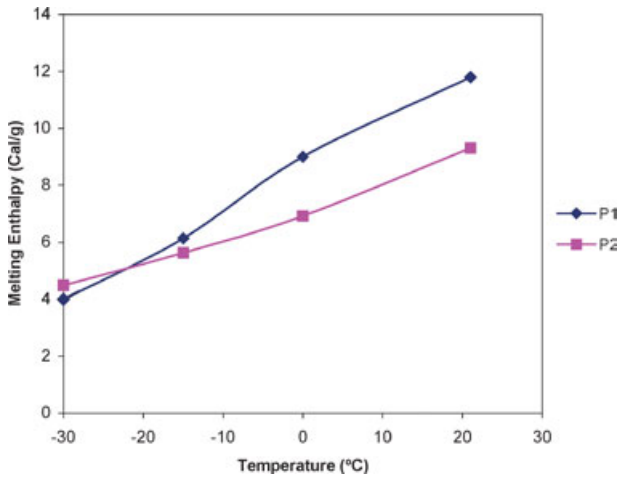

FIGURE 10. Melting enthalpy of the first crystalline region with temperature of deformation for single-screw extruder (P1) and twin-screw extruder (P2) procedures.

−100 to 250°C under nitrogen. Results are shown in Fig. 9 for the pure EVA as received (second line from top) and those with the thermal treatment (third line from top). As observed, the first endotherm at 48°C is absent in the third line. As the sample is quenched, the contribution from the first crystalline region vanishes.

The melting enthalpy decreases with mixing intensity (twin-screw extruder) in the preparation of the samples and augments with temperature of deformation as is shown in Fig. 10. It is also observed that the melting enthalpy of the first crystalline region increases with deformation. In Fig. 11, the melting enthalpy is plotted with EVA content for both, the undeformed samples and deformed samples at break point. Preparation process of the blends included previous mixing in a twin-screw extruder. Figure 11 clearly shows the effect of molecular ordering and increase strain induced crystallization on the melting enthalpy. In addition, glass transition temperatures of EVA (−37°C) and PP(−11°C) are not substantially affected in the blends, a very small variation occurs in the melting temperatures of EVA (76°C) and PP (173°C) around 4°.

COMPATIBILIZED BLENDS

The infrared spectrum for PPMA, EVAOH, and their blends are shown in Fig. 12. The spectrum from the EVAOH has a broad peak in the region between 3500 and 3200 cm^{-1} typical for polymeric alcohols.[43] In the spectrum after blending both copolymers in a proportion 1:1 mol, that peak is not present. This suggests the reaction between the OH of the EVAOH and the carbonyl group of the maleic anhydride in the PPMA.

During the mold injection process, the blends with PPMA and EVAOH can be processed at lower injection pressures (from 7.2×10^5 to 6.2×10^5 Pa). In Fig. 13, it was observed that in the samples without compatibilizer, lateral contraction is larger after the molding process, and the size of bubbles is also larger.

Blends for these studies were prepared by extrusion with a twin-screw extruder followed by a second extrusion cycle in a single-screw extruder

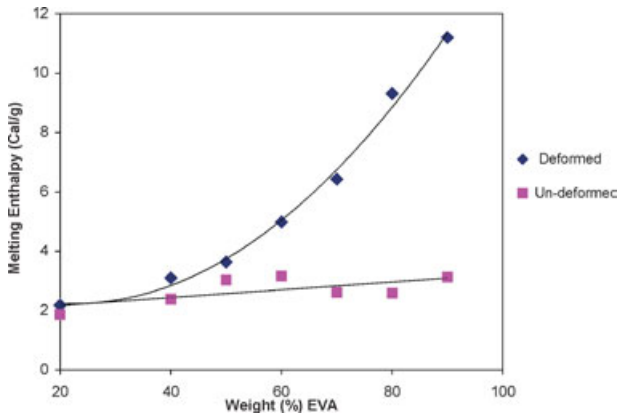

FIGURE 11. Melting enthalpy of the first crystalline region with EVA content for deformed (D) samples at room temperature and undeformed samples (UD).

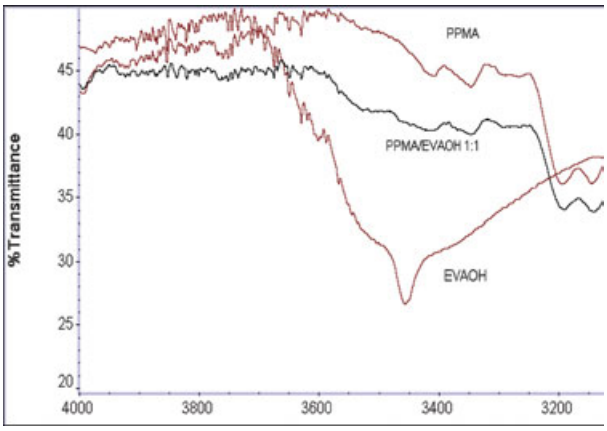

FIGURE 12. Upper spectrum: PPMA. Middle spectrum: after blending both compatibilizers in a proportion 1:1 molar. Lower spectrum: EVAOH.

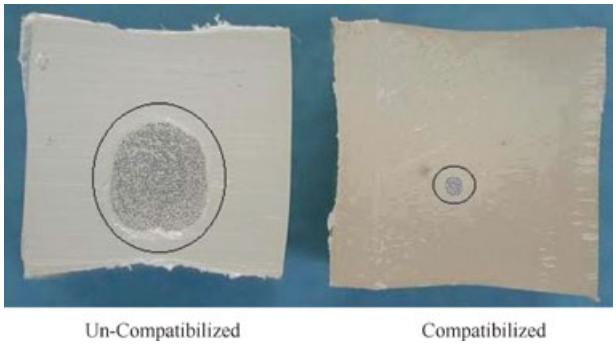

FIGURE 13. Photographs of impact samples show a larger contraction and bubble size in the 80/20 uncompatibilized sample.

before the injection molding process. The morphology of samples obtained in the 80/20 PP/EVA system (Fig. 14a) and the blend with 6.2 phr of PPMA + EVAOH content (Fig. 14b) reveal that the domain size decreased from 1.5 to 1 μm with the addition of the compatibilizer. For this comparison, the maximum domain size in two dimensions from the micrographs was considered. As the EVA content is increased to 40%, with 6.2% of compatibilizer, it is clear that the interface adhesion is improved greatly in the blend with PPMA + EVAOH as shown in Fig. 14d as compared to that shown in Fig. 14c without compatibilizer.

After etching the EVA phase with toluene, the morphology of the 60/40 and 50/50 PP/EVA blends is shown in Fig. 15. In the case of the blend 60/40 with PPMA + EVAOH, the domain size of the dispersed phase is very small (around 0.1 μm) as clearly observed in Fig. 15b. The morphology of this blend is compared to that shown in Fig. 15a, exhibiting profound differences attributed to the presence of the grafted compounds. At 50/50 PP/EVA content, the morphology becomes co-continuous, as shown in Fig. 15c. In the blends with compatibilizers, Fig. 15d shows the voids left after the EVA extraction. Finally, when PP is the dispersed phase, the addition of the grafted compounds also produces a reduction in the

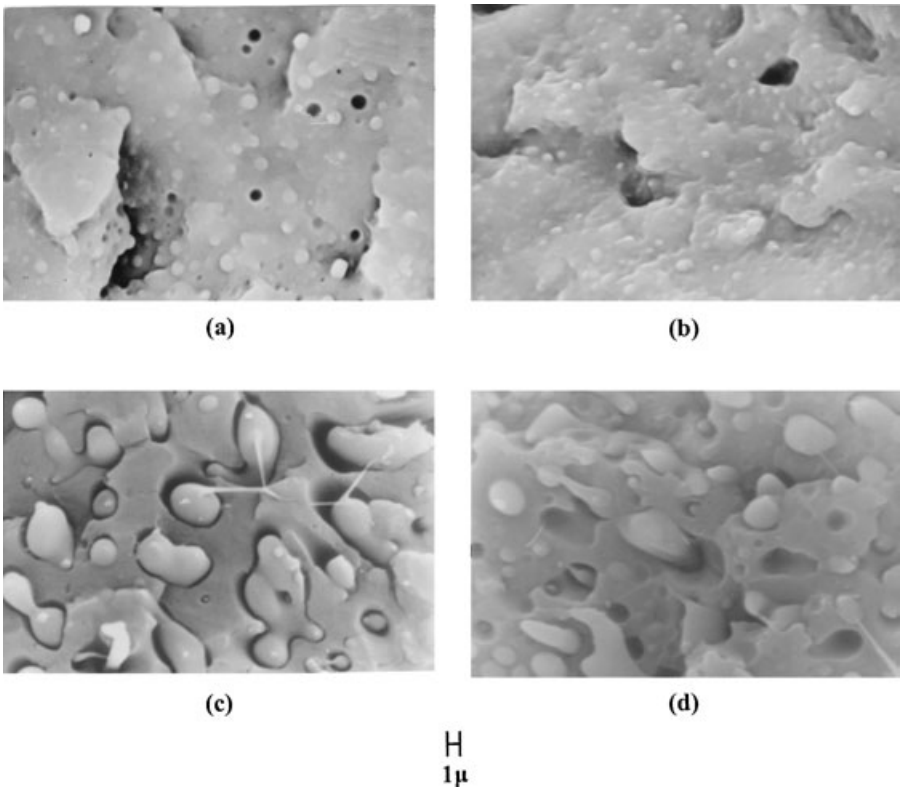

FIGURE 14. Morphology of the blends PP/EVA. (a) 80/20 uncompatibilized; (b) compatibilized; (c) 60/40 uncompatibilized; (d) compatibilized.

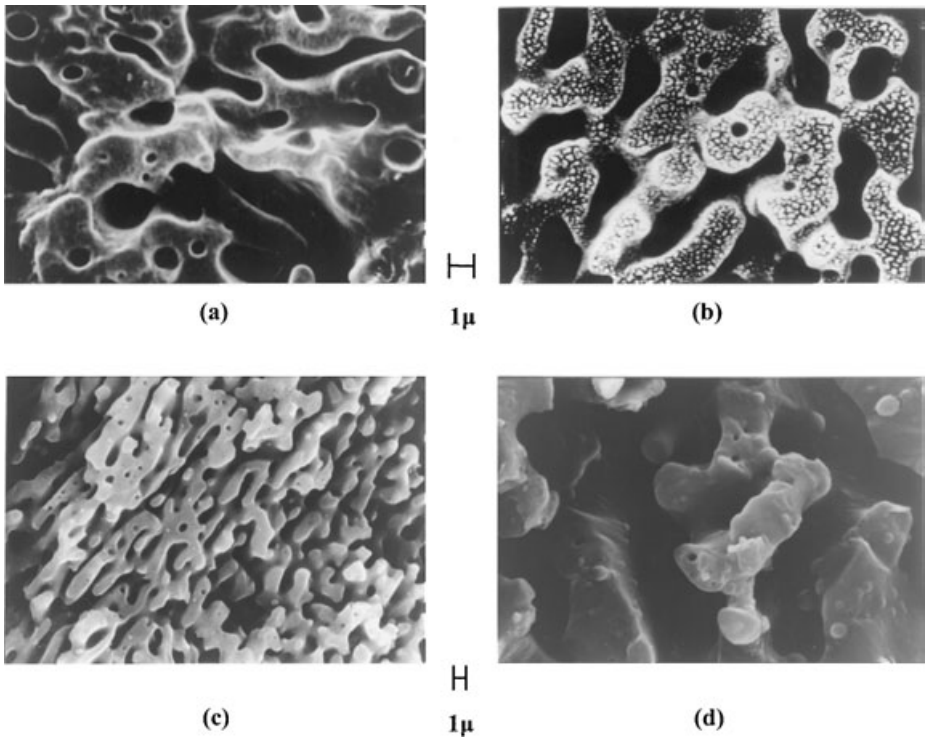

FIGURE 15. Morphology of the blends PP/EVA. (a) 60/40 uncompatibilized; (b) compatibilized; (c) 50/50 uncompatibilized; (d) compatibilized.

particle size, as observed in the comparison of micrographs in Figs. 16a and 16b.

Figures 17 and 18 show the impact resistance variation with particle size. In Fig. 17, impact resistance increases linearly with particle size as the EVA content is increased, when the compatibilizers content is 6.2 phr. However, for the same EVA content, the presence of PPMA + EVAOH induces a reduction in the particle size that is related to an increase in the impact resistance, as observed in Fig. 18.

Impact properties of the blends are substantially modified with the addition of PPMA and EVAOH.

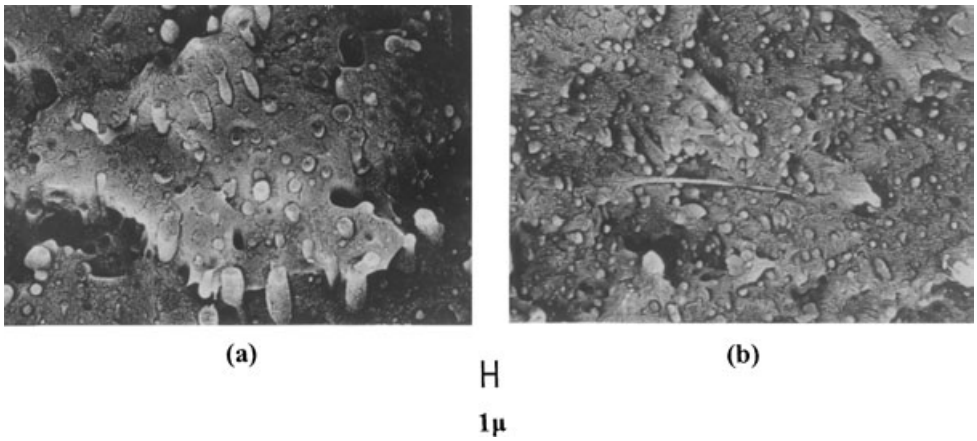

FIGURE 16. Morphology of the blends PP/EVA. (a) 20/80 uncompatibilized; (b) compatibilized. A reduction in the domain size is observed.

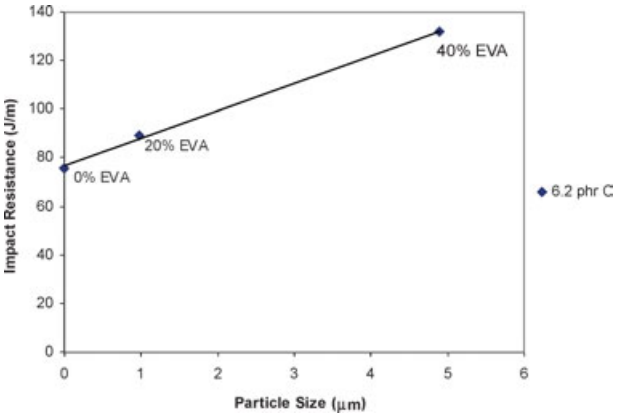

FIGURE 17. Impact resistance versus particle size for compatibilized blends.

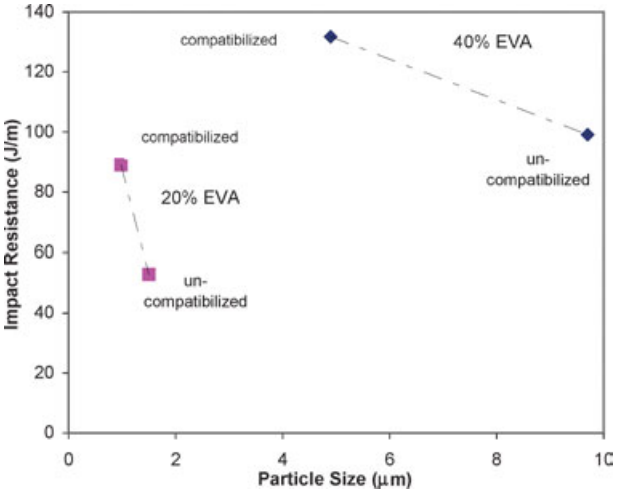

FIGURE 18. Impact resistance versus particle size for compatibilized and uncompatiblilized blends. The dotted lines join the two points of the blends to compare, with same concentration of PP/EVA.

In Figs. 19 and 20, the impact resistance is plotted with EVA content for the systems studied in the micrographs at two temperatures (room temperature, Fig. 19 and −30°C, Fig. 20). At room temperature, an improvement in the impact resistance is observed when the grafted compounds content is 6.2 phr for low EVA concentrations. As the EVA content is increased to more than 40%, a higher proportion of the compatibilizer is needed to achieve better impact resistance. Same conclusions are met when the temperature is −30°C, as shown in Fig. 20. However, the remarkable increase in the impact resistance obtained for low EVA concentrations with the addition of 6.2 phr of the grafted compounds is superior to that at room temperature.

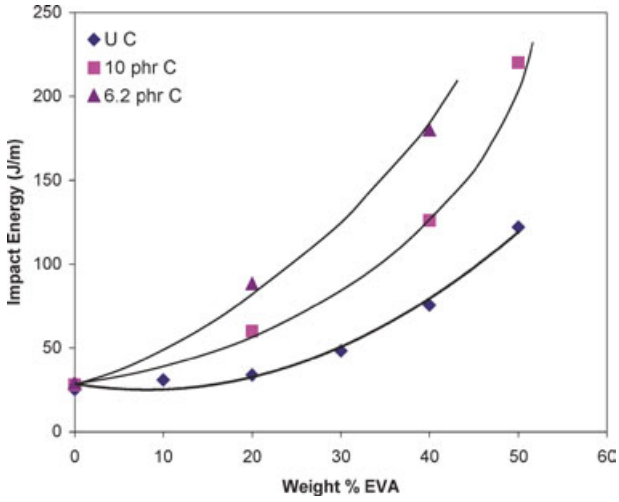

FIGURE 19. Impact resistance with EVA content at room temperature for compatibilized ((C) 6.2 phr and 10 phr) and uncompatibilized (UC) blends.

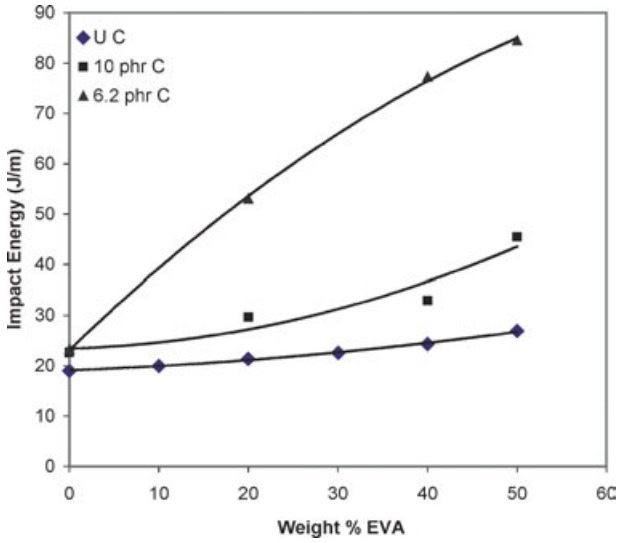

FIGURE 20. Impact resistance with EVA content at −30°C for compatibilized ((C) 6.2 phr and 10 phr) and uncompatibilized (UC) blends.

Conclusions

This study has shown the substantial modification in the morphology of the PP/EVA blends caused by the addition of grafted PP and hydroxylated EVA. In particular, a relationship was found between the impact resistance and both EVA concentration in the

blend and particle size of the dispersed EVA phase. This relationship was directly related to changes in the microstructure due to the presence of the compatibilizing compounds. For example, for an EVA content of 40% in the blend, an increase of more than 270% in the impact resistance is obtained with the addition of 6.2 phr of compatibilizers at room temperature (see Fig. 19). Figure 14d clearly shows that the effect of the addition of the grafted compounds is to improve the interfacial adhesion of the particles to the matrix for this system. Furthermore, for the same EVA content, if we increase the compatibilizer content to 10 phr, an additional rise in the impact resistance is obtained. Similarly, this result follows from the decrease in the particle size as observed in Fig. 15b.

With respect to the tensile properties of the PP/EVA blends at low temperatures and large EVA content, the peak in the stress versus deformation curves is related to the deformation of the domains of PP in the initial region of the curves, which is characteristic of pure PP. At room temperature, this relation is weak, since the domains are not greatly deformed.

The melting enthalpy is increased with rising crystallinity under tension in the first crystalline region of the EVA copolymer, and with rising temperature of the test.

Acknowledgments

Authors would like to thank Ernesto Sánchez, José Guzmán, Antonio Sánchez, Miguel Angel Canseco, Fernando Silvar, Sara Jimenez, Ma. Teresa Vázquez, J. Jesus Camacho, Juan Manuel García Leon, and Antonio Caballero for their technical support and to students Edgar Sanchez and Ma. Trinidad Reynoso.

References

1. Kargez, J.; Kuleznev, U. N. Polymer 1982, 23, 699.
2. Van der Wal, A.; Nojhof, R.; Gaymans, R. J. Polymer 1999, 40, 6031.
3. Van der Wal, A.; Gaymans, R. J. Polymer 1999, 40, 6067.
4. Kim, J. Y.; Chun, B. C. J Mater Sci 2000, 35, 4833.
5. Jang, B. Z.; Ulmann, D. R.; Vander Sade, J. B. Polym Eng Sci 1985, 25, 643.
6. Van der Wal, A.; Verheul, A. J. J.; Gaymans, R. J. Polymer 1999, 40, 6057.
7. Jiang, W.; Tjong, S. C.; Li, R. K. Polymer 2000, 41, 3479.
8. Coppola, F.; Greco, R.; Martuscelli, E. Polymer 1987, 28, 47.
9. Greco, R.; Mancarella, C.; Martuscelli, E.; Ragosta, G.; Jinghua, Y. Polymer 1987, 28, 1929.
10. D'Orazio, L.; Mancarella, C.; Martuscelli, E.; Sticotti, G.; Massari, P. Polymer 1993, 34, 3671.
11. Gupta, A. K.; Purwar, S. N. J. Appl Polym Sci 1986, 31, 535.
12. Thomas, S.; Gupta, B. R.; De S. K. Polym Degrad Stab 1987, 18, 189.
13. Thomas, S. Mater Lett 1987, 5, 360.
14. Jafari, S. H.; Gupta, A. K. Appl Polym Sci 2000, 78, 962.
15. Gallego Ferrer, G.; Salmerón Sánchez, M.; Verdú Sánchez, E.; Romero Colomer, F.; Gómez Ribelles, J. L. Polym Int 2000, 49, 853.
16. Thomas, S.; George, A. Eur Polym J 1992, 28, 1451.
17. Ramírez-Vargas, E.; Navarro-Rodríguez, D.; Medellín-Rodríguez, F. J.; Huerta-Martínez, B. M.; Lin, J. S. Polym Eng Sci 2000, 40, 2241.
18. Wang, Z. J Appl Polym Sci 1996, 60, 2239.
19. Khastgir, D.; Ray, I. Polymer 1993, 34, 2030.
20. Duvall, J.; Sellitti, C.; Myers, C.; Hiltner, A.; Baer, E. J Appl Polym Sci 1994 52, 207.
21. Rôsch, J.; Mulhaûpt, R. J Appl Polym Sci 1995, 56, 1599.
22. Re-produced from Modern Plastics Magazine. McGraw-Hill by Revista de Plásticos Modernos 1991, 251.
23. Zhang, X. M.; Yin, J. H. Polym Eng Sci 1997, 37, 197.
24. Liang, Z.; Williams, H. L. J Appl Polym Sci 1992, 44, 699.
25. Kim, B. C.; Hwang, S. S.; Lim, K. Y.; Yoon, K. J. J Appl Polym Sci 2000, 78, 1267.
26. Mehrabzadeh, M.; Nia, K. H. J Appl Polym Sci 1999, 72, 1257.
27. Dutra, R. C. L.; Soares, B. G.; Gorelova, M. M.; Silva, J. L. G.; Lourenco, V. L.; Ferreira, G. E. J Appl Polym Sci 1997, 66, 2243.
28. Schoeder, K.; Klee, D.; Höcker, H.; Leute, A.; Benninghoven, A.; Mittermayer, C. J Appl Polym Sci 1995, 58, 699.
29. González-Montiel, A.; Keskkula, H.; Paul, D. R. Polymer 1995, 36, 4621.
30. Muratoglu, O. K.; Argon, A. S.; Cohen, R. E. Polymer 1995, 36, 921.
31. Kim, G. M.; Michler, G. H. Polymer 1998, 39, 5699.
32. Xiao, K.; Ye, L. Polym Eng Sci 2000, 40, 70.
33. Liu, Z.; Zhu, X.; Wu, L.; Li, Y.; Qi, Z.; Choy, C.; Wang, F. Polymer 2001, 42, 737.
34. Bazhenov, S. Polym Eng Sci 1995, 35, 813.
35. Ortiz Alba, E. M. Sc. Thesis, School of Chemistry, UNAM, Mexico, 1993.
36. Flores, M.; Hernandez, G.; Escobar, A.; Cardoso, J.; Palma, A.; Maciel, A.; Sánchez, E.; Manero, O. J Appl Polym Sci 1998, 47, 1071.
37. Maciel, A.; Sánchez, E.; Guzmán, J. Memories Polymex 93, International Symposium of Polymers, 1993; p. 247.
38. Young, R. J. Introduction to Polymers; Chapman and Hall: London, 1981.
39. Hay, I.; Keller, A. Kolloid Z Z Polym 1965, 204 (1/2), 43–74.
40. Manson, J. A.; Sperling, L. N. Polymer Blends and Composites; Plenum: New York, 1986.

41. Gupta, A. K.; Rana, S. K.; Deopura, B. L. J Appl Polym Sci 1993, 49, 477.
42. Jandali, M. Z.; Widman, G. Collected Applications. Thermal analysis; Mettler–Toledo: Schwerzenbach, Switzerland, 1999; pp. 1–56.
43. Pretsch, E.; Clerc, T.; Seibl, J.; Simon, W.; Tablas para la Elucidación de Compuestos Orgánicos por Métodos Espectroscópicos. Alhambra Madrid, 1985; p. I 90. Translated from "Tabelen Zur Strukturaufklarung Organischer Verbindungen Mit Specktroskopischen Metoden"; Springer-Verlag: Berlin, 1976.